Transformation of a Simple Plastic into a Superhydrophobic Surface

H. Yildirim Erbil, *et al.*

Science **299**, 1377 (2003);
DOI: 10.1126/science.1078365

and its frequency must be 30 cm^{-1} higher in the $v = 1$ bend levels than in their ground states. A frequency shift of this type would be another example of the breakdown of the harmonic picture in $H_5O_2^+$.

In the 4D vibrational calculations, the asymmetric stretch was predicted to be more than three times more intense than the two bending bands in $H_5O_2^+$, which does not agree well with the experimental spectrum. This discrepancy can arise from at least two factors: (i) The calculations refer to the linear absorption spectrum, whereas the photoinduced vibrational predissociation mechanism (Eq. 1) governing our IRMPD experiments requires the absorption of multiple photons (6 to 18 photons in the frequency range studied). The absorption of the first few photons within the discrete (in contrast to quasi-continuum) regime (*21*, *22*) generally governs the relative intensities observed in the IRMPD spectrum. Meijer and co-workers have found satisfactory agreement between the IRMPD and linear absorption spectrum for bi- and tricyclic hydrocarbon cations even though as many as 100 photons are required for dissociation (*23*, *24*). However, these ions are larger than the protonated water dimer, and there may be more deviation from the linear absorption intensities over the spectral range probed by our experiment if more photons are needed to reach the quasi-continuum, a particular concern at the lowest frequencies in Fig. 1. (ii) Anharmonic coupling to vibrational modes other than the four $O\cdots H^+\cdots O$ vibrations was not included in these calculations. The multiconfigurational self-consistent field calculations of Muguet (*15*) indicate that coupling to the water wags and bends is important. The fine structure in the experimental spectrum shows evidence for this type of coupling, which is likely to alter the overall intensity pattern.

The present results provide previously unstudied insight regarding the assignment of the liquid-phase spectra (*12*, *31*). Hydrated protons in aqueous solution are characterized by four broad absorption bands at 1200, 1760, 2900, and 3350 cm^{-1} and a continuous absorption over the 1000 to 3400 cm^{-1} range. In heavy water, the spectral features are red-shifted to 920, 1420, 2130, and 2480 cm^{-1}. On the basis of a comparison with the gas-phase spectra, the absorption of the hydrated proton (deuteron) in the 1200 and 1760 cm^{-1} (920 and 1420 cm^{-1}) region can be attributed to the presence of $H_5O_2^+$-type structures in the aqueous solution. The bulk 1760 cm^{-1} absorption is attributed to the blue-shifted bend vibration of the terminal water, which is found at 1741 cm^{-1} in the present gas-phase spectrum. This result confirms the original assignment of Librovich *et al.* (*11*) and recent multistate empirical valence-bond simulations by Kim *et al.* (*12*). The broad 1200 cm^{-1} absorption is attributed to three modes, namely the asymmetric stretch and the two bend modes of the $O\cdots H^+\cdots O$ moiety, that we find in the 920 to 1320 cm^{-1} region. We note that the liquid-phase difference spectra also show a very weak absorption at around 750 cm^{-1} and that a similar absorption is observed in our spectra at 788 cm^{-1} (band a).

References and Notes

1. M. Saraste, *Science* **283**, 1488 (1999).
2. J. K. Lanyi, *J. Phys. Chem. B* **104**, 11441 (2000).
3. R. Pomès, B. Roux, *Biophys. J.* **82**, 2304 (2002).
4. A. M. Smondyrev, G. A. Voth, *Biophys. J.* **82**, 1460 (2002).
5. M. Eigen, L. D. Maeyer, *Proc. R. Soc. London* **247**, 505 (1958).
6. C. J. T. d. Grotthuss, *Ann. Chim. (Paris)* **58**, 54 (1806).
7. J. D. Lear, Z. R. Wasserman, W. F. DeGrado, *Science* **240**, 1177 (1988).
8. N. Agmon, *Chem. Phys. Lett.* **244**, 456 (1995).
9. D. Marx, M. E. Tuckerman, J. Hutter, M. Parinello, *Nature* **397**, 601 (1999).
10. G. Zundel, *Adv. Chem. Phys.* **111**, 1 (2000).
11. N. B. Librovich, V. P. Sakun, N. D. Sokolov, *Chem. Phys.* **39**, 351 (1979).
12. J. Kim, U. W. Schmitt, J. A. Gruetzmacher, G. A. Voth, N. E. Scherer, *J. Chem. Phys.* **116**, 737 (2002).
13. L. I. Yeh, J. D. Myers, J. M. Price, Y. T. Lee, *J. Chem. Phys.* **91**, 7319 (1989).
14. L. I. Yeh, Y. T. Lee, J. T. Hougen, *J. Mol. Spectrosc.* **164**, 473 (1994).
15. F. F. Muguet, *J. Mol. Struct.* **368**, 173 (1996).
16. E. D. Valeev, H. F. Schaefer III, *J. Chem. Phys.* **108**, 7197 (1998).
17. K. R. Asmis *et al.*, *Phys. Chem. Chem. Phys.* **4**, 1101 (2002).
18. G. M. H. Knippels, R. F. X. A. M. Mols, A. F. G. van der Meer, D. Oepts, P. W. van Amersfoort, *Phys. Rev. Lett.* **75**, 1755 (1995).
19. M. Putter, G. von Helden, G. Meijer, *Chem. Phys. Lett.* **258**, 118 (1996).
20. N. L. Pivonka *et al.*, *J. Chem. Phys.* **117**, 6493 (2002).
21. S. Mukamel, J. Jortner, *J. Chem. Phys.* **65**, 5204 (1976).
22. A. S. Sudbo, P. A. Schulz, E. R. Grant, Y. R. Shen, Y. T. Lee, *J. Chem. Phys.* **70**, 912 (1979).
23. J. Oomens, A. J. A. van Roij, G. Meijer, G. von Helden, *Astrophys. J.* **542**, 404 (2000).
24. J. Oomens, G. Meijer, G. von Helden, *J. Phys. Chem. A* **105**, 8302 (2001).
25. Y. K. Lau, S. Ikuta, P. Kebarle, *J. Am. Chem. Soc.* **104**, 1462 (1982).
26. L. Ojamäe, I. Shavitt, S. J. Singer, *Int. J. Quantum Chem. Symp.* **29**, 657 (1995).
27. M. V. Vener, O. Kühn, J. Sauer, *J. Chem. Phys.* **114**, 240 (2001).
28. B-CCD(T) is the Brueckner coupled cluster doubles method with a perturbational triple-excitation correction. TZ2P is the triple-ζ plus double polarization basis set.
29. G. M. Chaban, J. O. Jung, R. B. Gerber, *J. Phys. Chem. A* **104**, 2772 (2000).
30. D. J. Wales, *J. Chem. Phys.* **110**, 10403 (1999).
31. R. Vuilleumier, D. Borgis, *J. Chem. Phys.* **111**, 4251 (1999).

32. Supported by the Collaborative Research Center 546 and the Ph.D. Graduate Study Program 788 of the Deutsche Forschungsgemeinschaft. U.S. Air Force Office of Scientific Research grant F49620-00-1-0018 provided support for N.L.P. and D.M.N. We thank M. V. Vener and J. Sauer for helpful discussions, the Stichting voor Fundamenteel Onderzoek der Materie for providing the required beam time on FELIX, and the FELIX staff, in particular A. F. G. van der Meer, for skillful assistance.

18 December 2002; accepted 29 January 2003
Published online 4 January 2003;
10.1126/science.1081634
Include this information when citing this paper.

Transformation of a Simple Plastic into a Superhydrophobic Surface

H. Yıldırım Erbil,[1]* A. Levent Demirel,[2]* Yonca Avcı,[1] Olcay Mert[1]

Superhydrophobic surfaces are generally made by controlling the surface chemistry and surface roughness of various expensive materials, which are then applied by means of complex time-consuming processes. We describe a simple and inexpensive method for forming a superhydrophobic coating using polypropylene (a simple polymer) and a suitable selection of solvents and temperature to control the surface roughness. The resulting gel-like porous coating has a water contact angle of 160°. The method can be applied to a variety of surfaces as long as the solvent mixture does not dissolve the underlying material.

Water repellency is important in many industrial and biological processes, such as the prevention of the adhesion of snow to antennas and windows, self-cleaning traffic indicators, the reduction of frictional drag on ship hulls, metal refining, stain-resistant textiles, and cell motility (*1, 2*). The hydrophobicity of a surface can be enhanced by a chemical modification that lowers the surface energy. This modification leads to an increase in the contact angle of a water drop, with a maximum value of approximately 120° reported for smooth CF_3-terminated surfaces (*2–5*). Superhydrophobic surfaces that have water contact angles larger than 150° have been obtained by controlling the surface topography of expensive hydrophobic materials by various processing methods, such as machining and etching (*1–12*). A superhydrophobic surface results from the increase of the surface roughness, so that the local geometry provides a large geometric area for a relative-

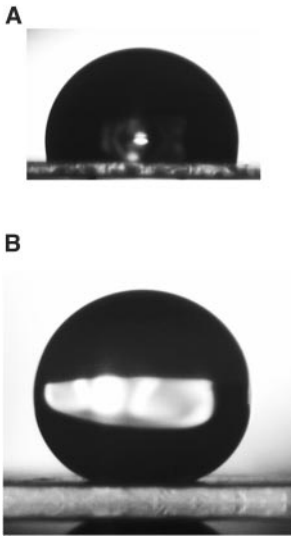

Fig. 1. (**A**) The profile of a water drop on a smooth i-PP surface that has a contact angle of 104° ± 2°. The i-PP film was prepared by melting at 200°C between two glass slides and crystallizing at 100°C. (**B**) The profile of a water drop on a superhydrophobic i-PP coating on a glass slide that has a contact angle of 160°. The i-PP was dissolved in a 60% p-xylene/40% MEK mixture by volume at an initial concentration of 20 mg/ml at 100°C. The solvent mixture was evaporated at 70°C in a vacuum oven. The morphology of the i-PP coating is shown in Fig. 4.

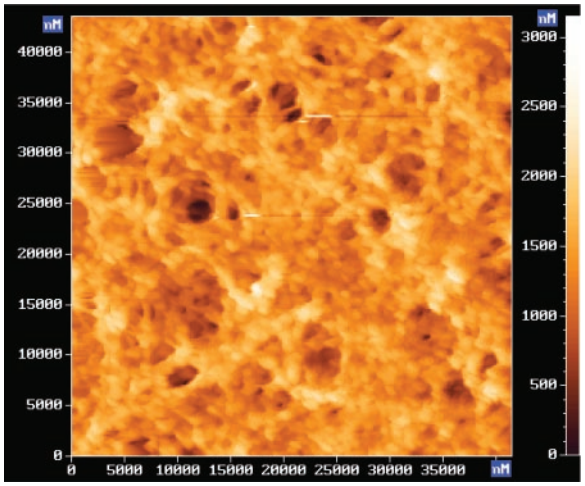

Fig. 2. AFM height image of an i-PP coating obtained from a solution (20 mg/ml) in p-xylene on a glass slide. The i-PP was dissolved in p-xylene at 130°C and solvent was evaporated in a vacuum oven at 70°C. The AFM image was taken in tapping mode using a silicon tip. The peak-to-peak roughness of the porous structure was 3200 nm, and the rms roughness was 300 nm.

ly small projected area. This effect can be observed in nature on the leaves of the sacred lotus (*13*, *14*). The surfaces of these leaves have micrometer-scale roughness, resulting in water contact angles up to 170°, because air that is trapped between the droplets and the wax crystals at the plant surface minimizes the contact area.

Isotactic polypropylene (i-PP), a commercially available hydrophobic polymer, has a melting temperature of 186° to 192°C and shows various morphologies, depending on the processing conditions. After melting i-PP between two glass slides at 200°C and subsequent crystallization at 100°C, we removed one of the glass slides and obtained a smooth surface. The roughness was checked with atomic force microscopy and had root mean square (rms) roughness of 10 nm. The shape of the water drop on the resulting surface had a contact angle of 104° ± 2° (Fig. 1A). To compare the water contact angle of films formed from melt with that of films prepared by solution casting, we prepared i-PP films by evaporating from p-xylene solvent at 130°C. These films showed banded spherulites and had a larger surface roughness of 40 nm, but the water contact angle was 105° ± 2°, still insufficient to be classified as superhydrophobic. We developed a new method for forming superhydrophobic coatings on a variety of surfaces using i-PP, and we improved the water contact angle value from 104° to 160° (Fig. 1B).

Porous polypropylene structures (or gels) are not new; they have been used in many contexts, including as porous polymer sorbents, membranes, and filters (*15*, *16*). For the gelation process, polypropylene is dissolved in a good solvent, such as o-xylene or decalin, and then the solution is either cooled or a nonsolvent, such as acetone or dimethyl formamide, is added to the solution before cooling, which results in spongy aggregates with diameters between 10 and 50 μm. The diameter decreases with the crystallization temperature. We modified this process to allow solvent casting of i-PP onto a wide variety of substrates by evaporating the solvent mixture, and we obtained a homogeneous film of porous gel-like structure.

We used p-xylene as a good solvent to dissolve granular i-PP. Methyl ethyl ketone (MEK), cyclohexanone, and isopropyl alcohol were investigated as the nonsolvent (the precipitator). The i-PP coating was obtained by dropping a few drops of the polymer solution onto glass slides and evaporating the solvent. The resulting i-PP coating had a white color. We have investigated the effect of polymer concentration (10 to 40 mg/ml), film formation temperature (30° to 90°C), and the nonsolvent on the homogeneity, surface roughness, and water contact angle of the i-PP coating. The coating was characterized by optical microscopy, atomic force microscopy (AFM), scanning electron microscopy (SEM), and contact angle measurements (*17*–*19*).

An AFM height image of the i-PP coating shows a porous morphology formed by a network of i-PP crystallites of different sizes and shapes (Fig. 2). Cylindrical bridges of i-PP connect the material on the two sides of the pores, resulting in a morphology that resembles a bird's nest made of branched and intermingled sticks and bumps. The coating is formed by rapid cooling from 130° to 70°C and relatively fast evaporation of p-xylene.

The peak-to-peak roughness of the coating is 3200 nm, and the rms roughness is 300 nm (Fig. 2). The increase in water contact angle with increasing surface roughness can be related to the two sources: the roughness factor, which is the ratio of the actual area to the projected area (*20*), and the air pockets formed by the microscopic pores, on which a substantial fraction of the water drop sits (*21*).

Raising the initial concentration of the polymer from 10 to 40 mg/ml increased the final coating thickness and the surface roughness, with contact angles increasing from 123° to 149°, respectively. Coatings obtained from solutions that had a concentration larger than 20 mg/ml had peak-to-peak roughness greater than the vertical limit of the AFM, which is 4000 nm. The surface morphology of such coatings was observed by SEM. The i-PP coatings obtained by casting onto glass slides from a solution of p-xylene increased the contact angle by ~40° as compared to smooth i-PP surfaces, but suffered from inhomogeneity as a drawback; there were cracks throughout the whole coating.

Changing the drying temperature and the drying conditions did not improve the homogeneity of the coatings, but it did add to our understanding of the mechanism of porous structure formation (Fig. 3). The solution at 130°C was dropped onto the glass slides in a vacuum oven at the specified drying temperatures, and the samples were kept in the vacuum oven at a constant temperature until the solvent fully evaporated. At the lower drying temperature, there was an increase in the inhomogeneity and size of the pores (Fig. 3, A and B) and also in the surface roughness and the contact angle, which varied between

[1]Department of Chemistry, Faculty of Sciences and Arts, Kocaeli University, 41300 İzmit, Kocaeli, Turkey. [2]Chemistry Department, College of Arts and Sciences, Koç University, Rumelifeneri Yolu, 34450 Sarıyer, İstanbul, Turkey.

*To whom correspondence should be addressed. E-mail: yerbil@kou.edu.tr (H.Y.E); ldemirel@ku.edu.tr (A.L.D.)

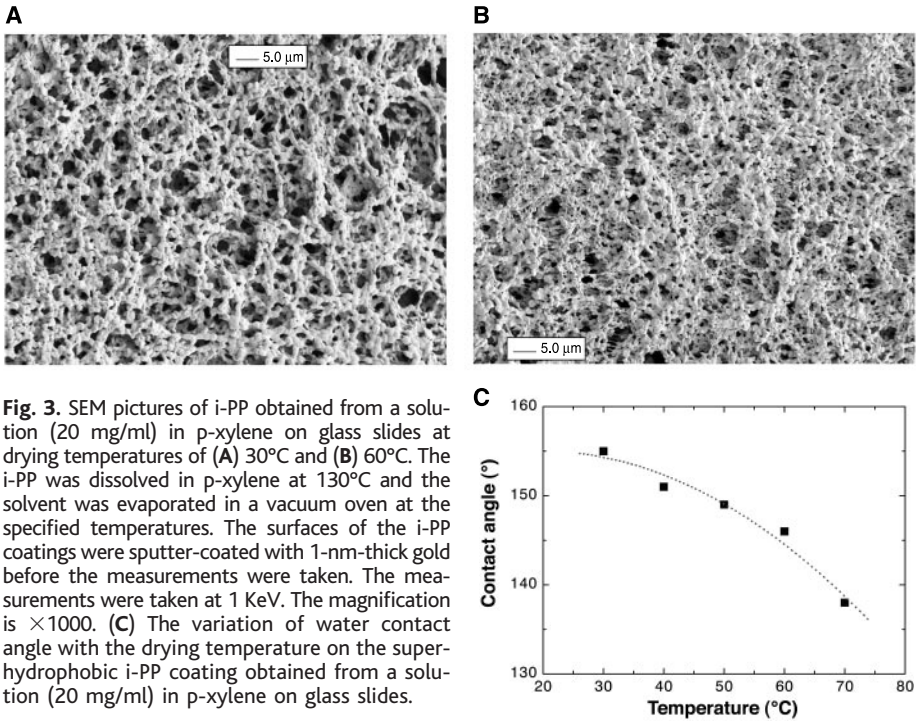

Fig. 3. SEM pictures of i-PP obtained from a solution (20 mg/ml) in p-xylene on glass slides at drying temperatures of (**A**) 30°C and (**B**) 60°C. The i-PP was dissolved in p-xylene at 130°C and the solvent was evaporated in a vacuum oven at the specified temperatures. The surfaces of the i-PP coatings were sputter-coated with 1-nm-thick gold before the measurements were taken. The measurements were taken at 1 KeV. The magnification is ×1000. (**C**) The variation of water contact angle with the drying temperature on the superhydrophobic i-PP coating obtained from a solution (20 mg/ml) in p-xylene on glass slides.

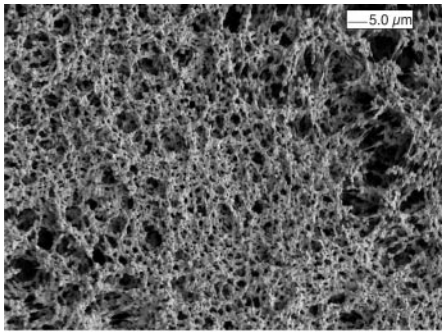

Fig. 4. SEM picture of an i-PP coating obtained using the nonsolvent MEK as described in Fig. 1B.

138° and 155° (Fig. 3C). As the temperature is decreased, the solvent evaporation rate is slower, and thus the crystallization time is increased, giving a higher overall crystallinity. However, the lower drying temperatures also increase the nucleation rate and pore formation, thus resulting in a loose network of coating morphology.

Mixing the good solvent p-xylene with a nonsolvent resulted in homogeneous coatings on glass slides over the whole area that was initially covered by the solution. Among the nonsolvents we have examined (MEK, cyclohexanone, and isopropyl alcohol), MEK gave the best homogeneity (Fig. 4) and the largest contact angle of 160° (Fig. 1B). Its high polar solubility parameter causes a stronger interaction with the hydroxyl groups on the glass substrate and results in better spreading of the i-PP solution. Compared to coatings obtained from the solvent only (Fig. 3B), coatings from the solvent/nonsolvent system of p-xylene/MEK have smaller i-PP crystallites and narrower cylindrical bridges (Fig. 4) with larger pores and a larger pore size distribution. On this superhydrophobic surface, the fraction of air in the pores in touch with the water drop is larger, and this fact accounts for the increase in water contact angle from 149° to 160°.

When nonsolvents are used in conjunction with p-xylene solvent, they have three impacts: (i) Nonsolvents act as a polymer precipitator by increasing the extent of polymer phase separation between the two phases of nonsolvent plus p-xylene and polymer plus small amount of p-xylene. This process decreases the crystallization time and gives smaller aggregates. The completion of this process leads to separation into two macroscopic phases: one polymer-rich and the other polymer-poor. Crystallization starts in the polymer-rich phase by the formation of crystal nuclei, with further development into spherulites, fibrilates, and other crystal shapes as seen in SEM images. The solvent then evaporates from these pores. (ii) The presence of the nonsolvents increases the nucleation rate, thus giving smaller spherulites. Also, because the nonsolvents are more volatile than the p-xylene, they increase the rate of evaporation and decrease the time needed for crystal formation. (iii) The addition of nonsolvents that contain oxygen increases the wettability of the polymer solution on the glass resulting from the presence of –OH groups on the substrate surface. This surface gives a homogeneous initial precipitate layer over which the network grows, forming a much more homogeneous final coating.

We also succeeded in forming superhydrophobic i-PP coatings on a wide variety of substrates other than glass slides, including aluminum foil, stainless steel, Teflon, high-density polyethylene, and polypropylene. The durability of the coatings on glass has been investigated (see supporting online text). The coatings did not debond when kept in water, in boiling water, or in heptane. The peel-off force in the normal direction was 0.13 ± 0.01 N. Although the free surface of the coating was porous, the back side facing the glass substrate was investigated by AFM and was found to have a smooth surface, indicating that the contact area between the film and the substrate is equal to the apparent area of the coating. No effect of compressive forces on the water contact angle was observed up to an average pressure of 5 MPa. The water contact angle decreased gradually beyond 5 MPa, down to 120° at a pressure of 500 MPa. The coatings maintained their superhydrophobicity between –20°C and the melting temperature, 160°C. Nanoscratch tests by AFM using a Si tip did not show any wear up to a normal force of 11.3 μN. Signs of contamination were not observed in coatings kept for 2 months in ambient atmosphere at relative humidity less than 40% and in the temperature range of 15° to 30°C.

For longer term applications, the adhesion to the underlying substrate can be further enhanced by standard techniques (*22*, *23*). The addition of superhydrophobicity to the well-known thermal and chemical stability of i-PP (*24*) may lead to new coating applications. When our SEM images are compared with SEM images of lotus leaves, we understand that we mimicked nature to find a simple solution for a difficult technological problem.

References and Notes

1. A. Nakajima, K. Hashimoto, T. Watanabe, *Monatsh. Chem.* **132**, 31 (2001).
2. S. R. Coulson, I. Woodward, J. P. S. Badyal, S. A. Brewer, C. Willis, *J. Phys. Chem. B* **104**, 8836 (2000).
3. W. Chen *et al.*, *Langmuir* **15**, 3395 (1999).
4. S. Veeramasuneni, J. Drelich, J. D. Miller, G. Yamauchi, *Prog. Org. Coat.* **31**, 265 (1997).
5. T. Nishino, M. Meguro, K. Nakamae, M. Matsushita, Y. Ueda, *Langmuir* **15**, 4321 (1999).
6. T. Onda, S. Shibuichi, N. Satoh, K. Tsujii, *Langmuir* **12**, 2125 (1996).
7. S. Shibuichi, T. Onda, N. Satoh, K. Tsujii, *J. Phys. Chem. B* **100**, 19512 (1996).
8. J. Bico, C. Marzolin, D. Quere, *Europhys. Lett.* **47**, 220 (1999).
9. D. Richard, D. Quere, *Europhys. Lett.* **48**, 286 (1999).
10. D. Oner, T. J. McCarthy, *Langmuir* **16**, 7777 (2000).
11. A. Hozumi, O. Takai, *Thin Solid Films* **334**, 54 (1998).
12. T. Tadnaga, N. Katata, T. Minami, *J. Am. Ceram. Soc.* **80**, 1040 (1997).
13. W. Barthlott, C. Neinhuis, *Planta* **202**, 1 (1997).
14. C. Neinhuis, W. Barthlott, *New Phytologist* **138**, 91 (1998).
15. G. P. Andrianova, S. I. Pakhomov, *Polym. Eng. Sci.* **37**, 1367 (1997).
16. H. Fujimatsu, Y. Ideta, H. Nakamura, H. Usami, S. Ogasawara, *Polym. J.* **33**, 543 (2001).
17. H. Y. Erbil, in *Handbook of Surface and Colloid Chem-*

istry, K. S. Birdi, Ed. (CRC Press Inc., Boca Raton, FL, 1997), chap. 9.
18. _____, G. McHale, M. I. Newton, *Langmuir* **18**, 2636 (2002).
19. Materials and methods are available as supporting material on *Science* Online.
20. R. N. Wenzel, *Ind. Eng. Chem.* **28**, 988 (1936).
21. A. B. D. Cassie, S. Baxter, *Trans. Faraday Soc.* **3**, 16 (1944).
22. R. A. Veselovsky, V. N. Kestelman, *Adhesion of Polymers* (McGraw-Hill, New York, 2002), chap. 2.
23. L. H. Sperling, *Polymeric Multicomponent Materials* (Wiley-Interscience, New York, 1997), chap. 6.
24. J. Varga, in *Polypropylene Structure, Blends and Composites*, J. Karger-Kocsis, Ed. (Chapman and Hall, London, 1995), vol. 1, chap. 3.
25. We thank A. Altay, M. A. Gülgün of Sabancı University, and A. Alkan of Brisa for their help with SEM measurements. A.L.D. acknowledges the financial support of the Turkish Academy of Sciences in the framework of the Young Scientist Award Program (grant EA/TÜBA-GEBİP/2001-1-1) and the Koç University Fiat Fund.

Supporting Online Material
www.sciencemag.org/cgi/content/full/299/5611/1377/DC1
Materials and Methods
Figs. S1 and S2
References

11 September 2002; accepted 22 January 2003

A New Species of Yunnanozoan with Implications for Deuterostome Evolution

Degan Shu,[1]* Simon Conway Morris,[2] Z. F. Zhang,[1] J. N. Liu,[1] Jian Han,[1] Ling Chen,[1] X. L. Zhang,[1] K. Yasui,[3] Yong Li[4]

Yunnanozoans are a distinctive clade of Lower Cambrian metazoans. Although widely accepted as deuterostomes, their exact placement within this superphylum is controversial. Here we describe a new species of *Haikouella* (*H. jianshanensis*) from the Chengjiang Lagerstätte (Yunnan, China) with exceptional preservation of a number of features. These include external gills, which suggest that the origin of the pharyngeal clefts was independent of the gills. The diagnostic branchial arches of chordates may, therefore, be composite structures. No evidence was found for the chordate-like structures that have been described in other yunnanozoans. We propose that yunnanozoans are stem-group deuterostomes, allied to the vetulicolians.

Yunnanozoans are a distinctive group of metazoans, occurring only in the Chengjiang fossil-Lagerstätte located near Kunming, in southwestern China (*1*, *2*). They are known from the type species *Yunnanozoon lividum* (*3*), *Haikouella lanceolata* (*4*), and *H. jianshanensis*, a new species described here. The body plan of yunnanozoans is defined by a relatively slender anterior bearing metamerically arranged gills and an expanded posterior section that dorsally bears a prominent segmented unit with a cuticular covering. Yunnanozoans have been described as deuterostomes but, alternatively, as some sort of stem group (*5*), hemichordates (*6*), cephalochordates (*7*), or craniates (*4*, *8*). These divergences of opinion have arisen on account of the distinctiveness of the yunnanozoan body plan and because postmortem crushing makes crucial details at the anterior difficult to discern (*3*, *4*, *6*, *8*). Here, on the basis of more than 1420 specimens of *Haikouella jianshanensis* (520 are well preserved), which predate the other two yunnanozoan species (*3*, *4*, *7*, *8*), we report a number of previously unidentified features.

The anatomy of *H. jianshanensis* differs from that of the other two known species in the size of the gills. Unlike other yunnanozoans (*3*, *4*, *5*–*8*), in which the dorsal segmented unit is well preserved, this region is only occasionally preserved (Fig. 1, A and B). Possibly, in *H. jianshanensis*, the cuticle was thinner, thereby decreasing the preservation potential of the posterior region. The anterior of the main body consists of two discrete units, dorsal and ventral, each in the approximate form of a compressed half cylinder (Fig. 1, G to J). These units are separated by a median zone (Fig. 1, A to F and K). The ventral unit is relatively robust and broadly canoelike, with a straight upper margin and recurved lower side. The dorsal unit has a more arcuate outline and is generally less well preserved, especially toward its posterior.

The cuticle of the median zone is thin and normally decomposed (Fig. 1, A to F, and Fig. 2, A to F), but occasionally, it survives as a smooth membrane (Fig. 2, G and H). The median zone generally decreases in height toward the posterior, which brings the dorsal and ventral units into juxtaposition; however, in different specimens, the overall width of this region is variable. The dorsal and ventral units are rarely touching (Fig. 1, G and H), suggesting that the entire anterior region could expand and contract in height. The expansion would occur by an accommodation along the median zone and about an axis of rotation near the posterior of the units.

A skirtlike structure runs around the entire anterior (Fig. 3, A to J) and is deflected outward and, to some extent, ventrally (*9*). The skirt consists of an upper barlike unit (Fig. 3, A and B), whereas the more ventral area is thinner but bears prominent dark lineations (Fig. 3, A, B, and G to J). The skirt is attached to the anterior ends of the ventral unit (on its mid-area), and the upper margin runs around the front end of the dorsal unit to which it may have been joined (Fig. 3, A and B). The lower part of the skirt hangs free (Fig. 3, G to J). In this configuration, the skirt defines a space between itself and the rest of the anterior body (Fig. 3, A, B, and E to H).

As in *H. lanceolata* (*4*), the gills of *H. jianshanensis* consist of six bilaterally symmetrical pairs, with each gill being inclined forward from its ventral insertion. In *H. jianshanensis*, the gills were robust structures, but the cuticle of the individual triangular leaves was thin enough for effective respiration (Fig. 2, C and D). At the anterior, they have an approximately sigmoidal configuration, but at the posterior, they tend to be more elongate. The gills were attached to the ventral unit, just dorsal to circular structures that may represent the proximal part of the gill or, alternatively, pharyngeal openings (Fig. 1, A to F; Fig. 2, A to F; and Fig. 3, K to N). Observations (*4*) on *H. lanceolata* were used to argue that the dorsal end of each gill was free and unattached, and in dorsoventrally compressed fossils of *H. jianshanensis*, the gills also bow outward; however, because of the angle at which such material was buried, it is not possible to determine the nature of the dorsal termination (Fig. 1, I and J, and Fig. 3, I and J). Evidence from laterally preserved specimens of *H. jianshanensis* for a dorsal attachment of the gills includes a consistent alignment with respect to the dorsal unit, and in specimens with an expanded median zone, the more widely separated dorsal and ventral units show straighter gills, especially in the anterior region (Fig. 1, A to F; Fig. 2, A to D; and Fig. 3, K to N). Each gill has a broad axis with transverse markings

[1]Early Life Institute and Department of Geology, Northwest University, Xi'an 710069, China, and School of Earth Sciences and Resources, China University of Geosciences, Beijing 100083, China. [2]Department of Earth Sciences, University of Cambridge, Downing Street, Cambridge CB2 3EQ, UK. [3]Institute of Molecular Embryology and Genetics, Division of Development and Biohistory, Kumamoto University, 2-2-1 Honjo, Kumamoto 860-0811, Japan. [4]College of Earth Science and Land Resources, Chang'an University, Xi'an 710054, China.

*To whom correspondence should be addressed. E-mail: elidgshu@nwu.edu.cn and dgshu@sein.sxgb.com.cn